18 October 1985, Volume 230, Number 4723 SCIENCE

Fluorescence Digital Imaging Microscopy in Cell Biology

Donna J. Arndt-Jovin, Michel Robert-Nicoud
Stephen J. Kaufman, Thomas M. Jovin

Summary. Developments in microscope, sensor, and image-processing technologies have led to integrated systems for the quantification of low-light-level emission signals from biological samples. Specificity is provided in the form of monoclonal antibodies and other ligands or enzyme substrates conjugated with efficient fluorophores. Fluorescent probes are also available for cellular macromolecular constituents and for free ions of biological interest such as H^+ and Ca^{2+}. The entire spectrum of photophysical phenomena can be exploited. Representative data are presented from studies of DNA conformation and architecture in polytene chromosomes and from studies of receptor-mediated endocytosis, calcium distribution, and the organization of the contractile apparatus in muscle cells.

The last few years have witnessed the increasing application of low-light-level (intensified) detectors, video image digitizers, and digital computers to basic research on biological specimens in the light microscope. These applications have ranged from the kinetic study of growth stimulation to three-dimensional (3D) image reconstruction of macromolecular assemblies in whole cells. A number of spectroscopic phenomena may be used for imaging in microscopes (Table 1).

This article focuses on fluorescence image analysis. Fluorescence imaging has a number of advantages for the study of biological objects (*1, 2*): (i) a particular macromolecule or cellular constituent can be selectively visualized in the presence of a great excess of other species; (ii) quantification is feasible at very low concentrations because of the inherent sensitivity associated with emission as opposed to absorption processes; (iii) low excitation intensities can be used to elicit a fluorescence signal, thereby preserving the viability of specimens under long-term observation; (iv) cellular components with dimensions below the diffraction-limited resolution of the light microscope can be visualized; (v) the intensity, excitation and emission spectra, and polarization state of emission can be exploited to assess the quantity, environment, mobility, and proximity of fluorophores used singly or in combination; and (vi) functional properties of cells and intracellular compartments, such as enzymatic activity (*3*), *p*H and membrane potential (*4*), ion and other small molecule fluxes (*5*), and the distribution and dynamics of intracellular organelles (*6*), can be measured with specific fluorescent probes and substrates.

Other recent advances have laid the basis for the field of digital microfluorimetric imaging of biological specimens. The first has been the development of sensitive and specific fluorescent probes for and analogs of biological macromolecules. The most widely applied of these probes are monoclonal antibodies (*7*) directly coupled to a fluorophore or used in conjunction with fluorescent secondary antibodies. Alternatively, fluorescent analogs (*8*) produced by direct conjugation of fluorophores to peptides or to subunits of macromolecules have been used in such studies as the assembly or disassembly of cytoskeletal components (*9*) and the dynamics of cell-surface receptor modulation (*6, 10*). It appears that fewer than 100 fluorophores can be detected if clustered so as to constitute essentially point sources (*6, 11*), thereby permitting visualization of a few or even single cell surface receptors. The limits of sensitivity can be extended with fluorophore complexes, such as the phycobiliproteins (*12*), that have quantum efficiencies and absorption extinction coefficients of more than $10^6 M^{-1}$ cm^{-1}. A second factor is the availability at moderate cost of fast arithmetic video processors and mass storage devices, as discussed below. Finally, there has been intensive development of microscope systems and sensors, particularly for use at the low light levels characteristic of biological systems or mandated by the need to avoid photodecomposition processes. Although image intensification systems have been evolving at a rapid pace for almost 20 years (*13*), it is only in the last decade that improvements in cost, availability, and performance have made them accessible to biologists.

Hardware Required for the Generation of Images

Clearly, the components that make up any specific system for what we designate Fluorescence Digital Imaging Microscopy (F-DIM) reflect the requirements of the individual research problems at hand. The following observations are therefore necessarily generalizations.

Optical microscopes. Recent advances in microscope design have reflected the advent of (i) new optical glasses; (ii) computer-aided optical design; (iii) computerized control systems; (iv) coherent stationary or scanned light sources in the form of continuous wave, modulated, and pulsed lasers; and (v)

D. J. Arndt-Jovin and M. Robert-Nicoud are senior staff scientists and T. M. Jovin is chairman of the Department of Molecular Biology, Max Planck Institute for Biophysical Chemistry, D-3400 Göttingen, Federal Republic of Germany. S. J. Kaufman is an associate professor in the Department of Microbiology, University of Illinois, Urbana 61801.

new optical train designs optimized for nonvisual sensing. However, the classic technologies have not been totally supplanted. Thus for many applications conventional arc lamp light sources are adequate or even essential, such as in experiments in the ultraviolet spectral domain. Modern microscopes tend to be modular with many alternative configurations of the objectives and stages. Inverted epi-illumination systems are increasingly favored, for example in situations where the simultaneous acquisition of electrophysiological and optical signals is desired. Linear or stepping motor control of focusing and stage motion have been extensively implemented in commercial and research instruments. Thus, a one-dimensional detector may be used to acquire 2D images, provided that the object, the light source, the detector, or the image (*14*) is mechanically scanned in the orthogonal direction (*15, 16*). Environmental control (*p*H, temperature, atmosphere, and medium) is an additional requirement in the case of viable biological samples.

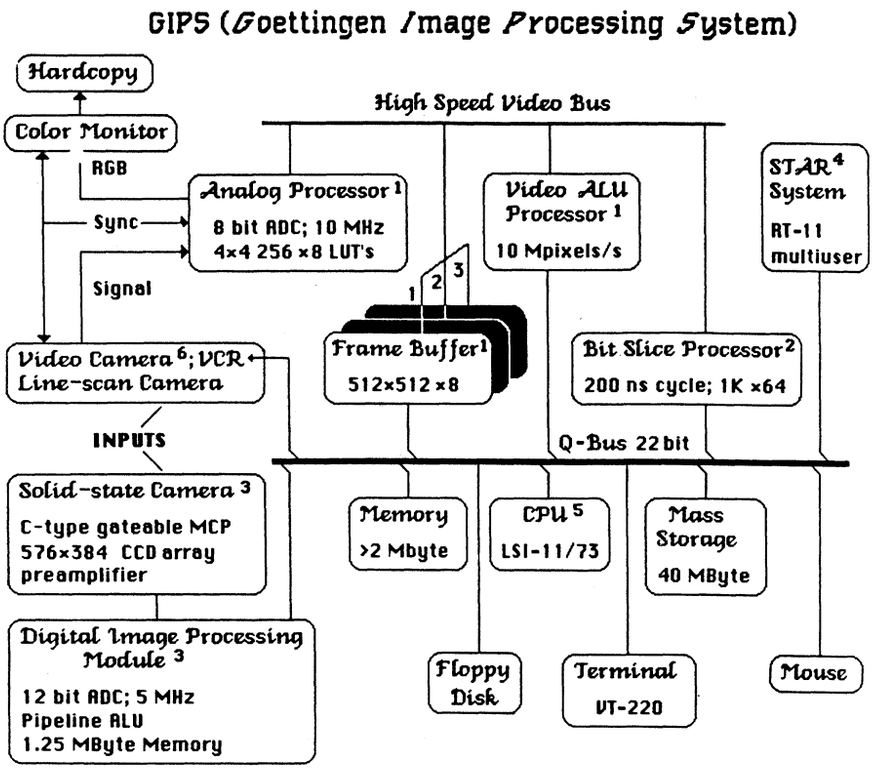

Fig. 1. Representative low-light-level image acquisition and processing system (GIPS). The input signals derive from either a TV source (video camera or video recorder) or a solid-state camera (line-scan or area-scan). In the case of the indicated (upper) inputs, an analog processor digitizes the signals and stores them in frame buffers with a resolution of 512 by 512 pixels per image or less. If desired, the digitized data can be subjected to real-time pixel transformations, such as contrast enhancement by nonlinear scale expansion at high or low video signal levels, through input-output tables (LUT). In addition, arithmetic operations (frame summation, exponential averaging, and subtraction) with a high-speed processor (ALU) can be performed before storage. Subsequent image processing is carried out using the combined resources of a microprocessor (LSI-11/73), the ALU, and/or a fast bit-slice processor under control of INCOS, an integrated hardware-software system. Other elements not indicated optimize synchronization and timing, control the operations of the video recorder, and map the Q-bus memory. Images can reside in the frame buffers, microprocessor memory (RAM), and on soft or hard disk (image files). The analog processor also generates a raster display (monochrome and/or color, RGB). A second independent camera system (at the time of this writing, not fully operational) consists of a CCD area detector coupled to a gateable (nanoseconds to seconds) MCP intensifier with an ultraviolet transmitting photocathode and a programmable electron gain of up to 5×10^5. The signals are preamplified, digitized with high resolution and speed (12 bits, 5 MHz), routed through a pipelined ALU, and stored in memory which is directly accessible from the microprocessor bus. In all cases, camera functions are under computer control, an essential feature for preventing damage to sensitive elements (intensifiers) and for establishing the required timing, synchronization, and gain. Suppliers (indicated by superscripts): (1) Imaging Technology Inc.: IP-512 family of image processing modules; (2) Signum: responsible for integration of the IP-512 modules, a bit-slice processor, the Q-bus system components, and appropriate software into a system (INCOS) capable of executing extensive menu-driven image acquisition and processing procedures both in real-time and from stored data; (3) Microtex Corp.: 4800 image intensifier system and 7405 digital processing system; (4) Hammond Software (STAR is a multiuser system based on DEC Q-bus or Unibus satellite processors in an RT-11 operating environment); (5) Digital Equipment Corp. (DEC) (the processor and other Q-bus components are from DEC or DEC-compatible vendors); (6) COHU Inc.: 4410 series double-intensified Newvicon TV camera.

An image from the optical microscope is a 2D projection of a 3D object. Several methods have been developed for obtaining a set of these projections from which the original object may be reconstructed. The most obvious (and effective) approach is to generate a set of 2D images at specified intervals in the focus axis (*15–18*). In a conventional microscope, these projections are acquired by successive movement of the object through the z axis. Standing-wave microscopy creates this set without mechanical movement of the stage by varying the spatial frequency of the excitation field (*19*). In laser scanning systems (*15, 16, 20–22*), the object is either transported mechanically, or it is scanned by a point source (the focused laser) and/or a point detector. The confocal configurations are particularly effective in diminishing out-of-focus contributions and scatter.

An important concern in quantitative microscopy is the use of systematic standards and procedures for evaluating system performance. Well-defined resolution and photometric targets and sources (fluorescent microspheres) are available (*23*). Nonetheless, the determination of resolution by evaluation of the modulation transfer function (MTF) remains a controversial matter (*24*). For example, the perceived spot image derived from a point source departs from the theoretical point spread function (psf) because of the physical effects of lens aberrations and diffraction in the optical train as well as complex distortions that reflect the local dielectric nature of the specimen itself (*25*). A frequent source of confusion is the spatial resolution attributable to self-luminescent (fluorescent) and thus incoherent sources in cytological material. That is, single protein (*11*) and DNA (*26*) molecules can be detected even though they have molecular dimensions far smaller than the diffraction-limited resolution imposed by the wavelength of the light (~0.2 μm). In this case, the "perception" of a discrete structure, as opposed to actual resolution, depends on the biochemical specificity of the labeling procedure, the local density of chromophores, the intensity of the excitation source, the efficiency of optical light collection and transfer, and finally the density and sensitivity (spectral and temporal) of resolution elements at final magnification in the image (detector) plane. Near-field scanning optical

microscopy (*27*) represents an attempt to achieve super-resolution (0.05 μm) with visible-wavelength radiation. Improvements of up to a factor of four in the spatial frequency bandwidth have been claimed for the confocal fluorescent microscope compared to the conventional configuration (*15*). Analytical image reconstruction methods have also been proposed as means for increasing resolution (*28*).

Other imaging systems. An elaboration of object scanning systems coupled to hydrodynamic fluid transport is represented by flow cytometers and sorters (*29*), in which cells traverse the site or sites of excitation and detection at high speed (*30*). These techniques achieve high statistical precision. Features dependent on orientation about the flow axis can be assessed with a system of orthogonal detectors, the spectral sensitivities of which can be adjusted for optimal discrimination. Microscope technologies based on physical phenomena other than light absorption and emission include the x-ray microscope (*16, 31*), the acoustic microscope (*16*), the photoelectron microscope (*32*), the ion microscope (*33*), and the electron microscope (transmission, scanning, and combinations with optical methods). A recent development has been that of the scanning tunneling electron microscope (*34*).

Detectors. Several reviews summarize the properties of sensitive and ultrasensitive (intensified) optical detectors suitable for fluorescence microscopy (*13, 35*). Physical laws dictate that the resolution of ideal sensors will be limited by the root-mean-square noise derived from photon statistics, particularly in the case of low-light-level systems with high-gain intensification stages. The signal-to-noise ratio (SNR) can be improved by intensification, image summation, and image enhancement operations. Thus, available spatial resolution is a function of light level and is variably specified in terms of line pairs, TV lines, or picture elements (pixels) per millimeter in the image plane. The highest resolution currently achievable in an area detector is on the order of 1500 by 1500 TV lines with Vidicon TV tube technology. Higher sensitivity but lower resolution is achieved with the following TV imaging tubes in current use: a silicon intensified target (SIT), an intensifier SIT (ISIT), and single-, double-, or even triple-intensified Vidicons, Newvicons, and Isocons. However, these first-generation devices are being challenged by the products of alternative detection and intensification technologies, particularly solid-state sensors.

Photoconductive solid-state detectors are generally based on charge-coupled devices (CCD), charge-injected devices (CID), and photodiode technologies. Linear arrays coupled to mechanical scanners can approach or exceed the resolution of the Vidicon, particularly as units with over 5000 elements become available. Two-dimensional solid-state arrays with 10^5 to 2×10^5 pixels are common; sensors with more than 10^6 pixels are in limited production. Solid-state detectors offer the significant advantages of geometric accuracy and stability, compactness, linearity, and freedom from lag, but they differ greatly with respect to uniformity of sensitivity, dark current, cross talk, readout noise, and the tendency to bloom or smear. Adherence to TV industry standards for frame rates and line scan formats can be detrimental for the purposes of image processing in microscopy. For example, a frequent consequence of the conventional 4:3 aspect ratio is that the pixels in the digitized image deviate from a "square" representation of object geometry.

For low-light-level applications, image intensification is usually required. Solid-state detectors are generally coupled by fiber optics or a relay lens to proximity-focused diodes and microchannel plate (MCP) intensifier tubes with adjustable, gateable gains of up to 10^4 to 10^5. Such systems can operate at an illuminance less than 10^{-6} lux and can accommodate image sizes of 18 mm or larger (*35*). An additional virtue of an intensifier section

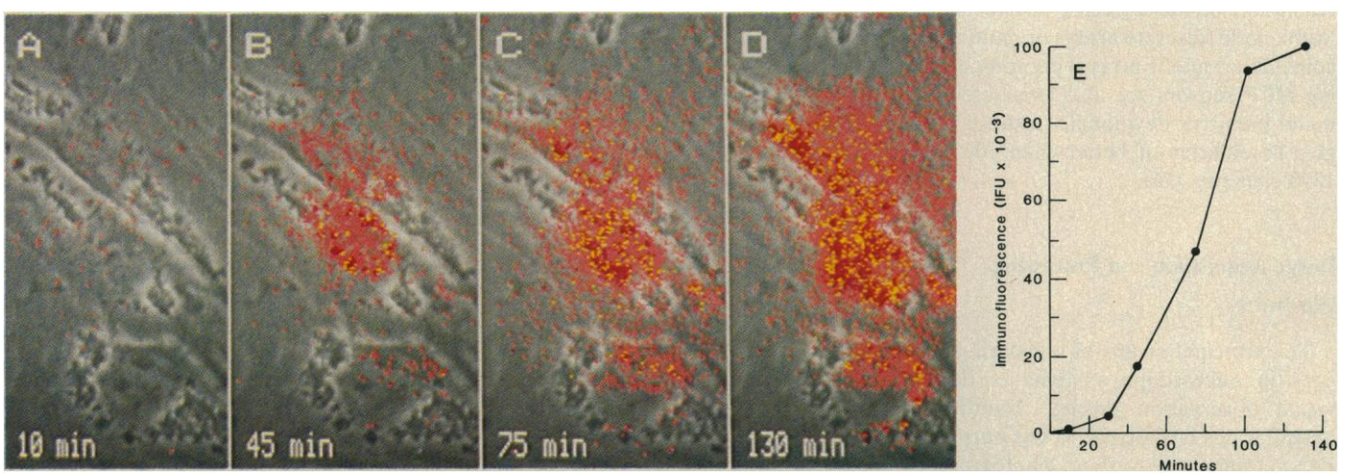

Fig. 2. The real-time uptake of rhodamine-labeled α_2-macroglobulin by E63 rat myoblasts in a 3-day confluent culture of cells undergoing developmentally regulated differentiation. Terminal differentiation is characterized by cell cycle G_1 arrest, the cessation of receptor-mediated α_2-macroglobulin uptake, and fusion into myotubes. The uptake and accumulation of rhodamine-labeled α_2-macroglobulin is visualized from 10 to 130 minutes at 22°C. The protein solution was 0.22 μ*M* in Hepes-buffered Dulbecco minimum essential medium without serum. Difference images displaying uptake were computed from (256 averaged) frames at each time point from which the zero-time image was subtracted to eliminate background, which in this case consisted largely of contributions from unbound fluorescent ligand. The latter produced a mean pixel value of 100 on the scale of 0 to 256 [the units of which are designated here integrated fluorescence units (IFU); it was estimated from measurements on standard solutions that 1 IFU was equivalent to about 33 α_2-macroglobulin molecules]. The difference fluorescence images are overlaid on the corresponding phase-contrast images. (A to D) Images obtained in the time interval of 10 to 130 minutes. Color coding (gray-level ranges): pink (0 to 47), yellow (48 to 63), red (64 to 255). (E) Quantitation of total uptake given by the integrated difference fluorescence images. The images were obtained with a Zeiss epi-illumination fluorescence microscope: oil immersion 63X objective [numerical aperture (NA), 1.4]; excitation, 546-nm bandpass plus 1.06 OD neutral density filter; emission, above 590 nm; COHU camera 4410 with GIPS acquisition (Fig. 1). Localization at earliest time is in the receptosomes, which progress at later times to the perinuclear lysosomal region. The upper two cells show linear uptake (30 to 100 minutes), whereas the cell in the lower third of the image shows extremely reduced uptake and is presumably more advanced in its differentiation.

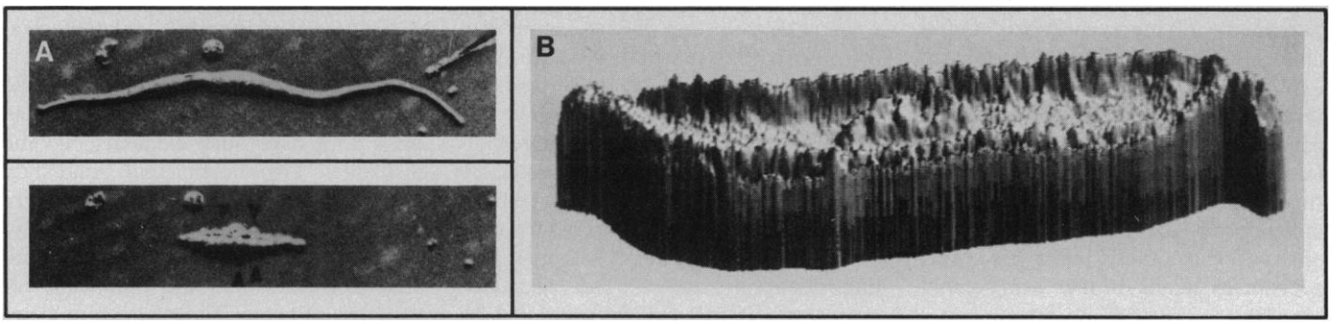

Fig. 3. Analysis of Ca^{2+} distribution in a single toad smooth muscle cell with a digital imaging microscope. (A) Two photomicrographs from a cine record taken with Normarski optics before (upper image) and after (lower image) extracellular electrical stimulation [data from Fay and Delise (*42*)]. Note the ability of the cells to shorten actively with formation of characteristic membrane evaginations (darts) associated with the process of contraction. (B) Contour plot of *p*Ca in a single living smooth muscle cell in the relaxed state from measurements of Fura2 fluorescence emission [data from Williams and colleagues (*5*)]. The image was created with a Lexidata graphics system with Lexidata solids display software.

is the extended spectral range it can provide (for example, into the ultraviolet region); optimal matching to the solid-state sensor can be achieved by judicious choice of phosphors. In a parallel development of ultrasensitive light sensors, the imaging capabilities of MCP intensifiers are exploited directly in the form of photoemissive array detectors (*36*). Thus at very low light levels single photons generate a discrete electron image, the coordinates of which are registered by integrated 2D position-sensitive detectors (resistive film anodes or wedge-and-strip arrays) or a coupled TV tube. The image is then generated by conventional 2D multichannel analysis. This mode of operation is not feasible at high light levels at which the pulse-pair temporal resolution of the detector is exceeded. Multianode (discrete arrays or multilayer coincidence anode arrays) photon-counting MCP sensors are also available and under intensive development; these may give resolutions of better than 1000 by 1000 elements (*36*).

Image Acquisition and Processing

Hardware

The principal means of registering images in microscope systems is direct visual observation through traditional optical trains optimized for this purpose. For permanent recording, photographic film is used extensively; the recent advent of fast black-and-white as well as color emulsions has facilitated applications involving extremely low light levels. However, film has several disadvantages: real-time signal processing is of course excluded, exposed film density bears a nonlinear and offset relation to incident light intensity, and spectral sensitivities are complex and often poor in the region of interest. Some of these limitations can be overcome by the judicious use of standardization procedures and digitizing hardware (flying-spot scanners and densitometers).

The future of quantitative microscopy, however, clearly lies with detectors producing images that can be directly visualized on a monitor and digitized in real-time or after an intermediate step of analog recording with a video or similar recorder. Because of the electronic bandwidths of TV cameras and even faster solid-state sensors with frame rates in the range of 1 kilohertz, the hardware required consists of combinations of relatively autonomous (but programmable) components operating at video (megahertz) frequencies and integrated into a computer-based system. An actual implementation, the Göttingen Image-Processing System (GIPS) currently used in our laboratory, is shown in Fig. 1. It and other similar systems emphasize versatility and efficiency in real-time operations and in analysis and manipulation of acquired images. An image resolution of 512 by 512 pixels is easily achieved at moderate cost. However, higher resolution will be required to exploit the new area sensors with 1000 by 1000 or 2000 by 2000 elements, as well as mechanically translated linear detectors (1000 to 5000 elements). The dynamic range (ADC bits) required in digitization is also a function of the sensor SNR characteristics. Thus few TV cameras, especially those equipped with noisy intensification stages, generate more than 8 bits (256 gray levels) of resolution, whereas selected solid-state sensors (for example, cooled CCD arrays) can achieve a dynamic range of 12 to 14 bits (4,000 to 16,000 gray levels), albeit generally at the sacrifice of readout rate. For dynamically changing biological samples generating low-light-level images, intensification is required to provide speed with adequate resolution. In Fig. 1, frame buffers with "depths" of 8 bits are designated. They can be stacked to improve the SNR characteristics in the case of relatively static images (for example, through frame summation), to form real-time difference images, and to implement arithmetic and filtering operations. The latter operations can be based on algorithms involving linear convolution or nonlinear data processing.

A good video display is an absolute requirement for image processing operations, including interactive modes of operation in the case of complicated 3D manipulations. Often, multiple monitors (color or monochrome) are used in combination to display intermediate images during a sequence. For permanent archival purposes, images are stored as files on digital media (magnetic disks, magnetic tape, or optical recording disks). In

Table 1. Optical phenomena used in microscopy and imaging (*51*).

Phenomenon	Reference
Absorption, interference, and scattering	(*52*)
Phase contrast	(*53*)
Birefringence and polarization	(*54*)
Reflection interference contrast	(*55*)
Differential interference contrast	(*56*)
Circular intensity differential scattering	(*57*)
Differential polarization	(*58*)
Asymmetric illumination contrast	(*59*)
Schlieren optics	(*60*)
Sideband edge enhancement	(*61*)
Resonance enhancement (nonlinear effects)	(*62*)
Fluorescence emission	(*1*, *2*)
Intensities (quantum yields)	(*63*)
Spectra (excitation-emission)	(*4*)
Polarization	(*64*)
Resonance energy transfer	(*65*)
Time-resolved emission (lifetimes)	(*66*)
Recovery after photobleaching	(*43*)
Total internal reflection	(*67*)
Near-field imaging	(*27*)
Polarized delayed fluorescence	(*68*)

biological applications, the need for large capacities and random access to image files is common. Numerous digital compression algorithms are available for reducing storage requirements.

A desirable feature in an image-acquisition system is dual-ported video memory, which can be randomly accessed from the high-speed video bus as well as from the bus of a convenient micro- or miniprocessor (RAM). Time-consuming image transfers are thereby minimized. In addition to image processing functions, a local processor system provides for easy implementation of essential camera control functions, for example stabilization of timing signals and surveillance of sensitive camera elements such as MCP intensifiers. Microscope functions that are also integrated directly or implemented with satellite control processors include autofocusing (*37*), stage motion, selection of optical components responsible for spectral analysis (filter wheels and detector multiplexers) and gain (zoom), shutter activation, and light source pulsing and modulation.

Considerably more elaborate systems than that shown in Fig. 1 are available and in use. However, it is important to distinguish between the requirements of an individual measuring station (for example, a microscope) and those of a central multiuser facility for non–real-time operations. In general, the latter would be equipped with a mainframe computer and a number of elaborate software packages for image manipulation and processing.

Image Acquisition and Processing Software

Image restoration. Operations on digital images can be classified according to a hierarchy of objectives (*28, 38*). In image restoration, one corrects for systematic errors in the electro-optical system, such as illumination inhomogeneities, background contributions, geometric and photometric (nonlinearity and shading) distortions of the sensor, focusing and defocusing, motion blurring, and lack of registration. Inverse filter operations are usually required to restore an undistorted true image. Image restoration algorithms can be more effective if the corresponding image-gathering systems are designed with optimized spatial bandwidth characteristics (*39*).

Image enhancement. In image enhancement, significant features of the image (object) are selectively emphasized by operations such as smoothing (noise suppression), thresholding contrast stretching, filtering, and geometric transformations.

Image-processing procedures (linear and nonlinear, arithmetic and logical) generally operate on individual images or pairs of images ("dyadic" operations) and either holistically and/or in cellular logic operations restricted to single pixel locations or neighborhoods. Special-purpose, highly integrated microcircuits and system architectures (*40*) with dramatic speed enhancements have been developed by means of parallel processing, which exploits pipelining or processor arrays (or both). Image-processing software is closely coupled to and dictated by the nature of the available hardware and the requirement for intuitive, facile, and interactive user interfaces. Algorithms for implementing basic operations are assembled into macro calls and sequential tree structures. Software transportability tends to be greater in the case of higher level image-processing programs that are relatively independent of the specific hardware.

Image analysis. Restored, possibly enhanced, images are analyzed according to the experimental objectives by the derivation of quantitative estimations of intensity (gray-value quantization), spatial distribution (2D and 3D reconstruction), or spatial-temporal characteristics corresponding to the phenomena listed in Table 1. Area, shape, color, and texture are classic descriptors for the objective representation of images but are not generally based on fluorescence phenomena. Under development are approaches to the technically demanding estimation of intermolecular distances and motions on cell surfaces [for example, by determining fluorescence lifetime, spectra, polarization, and resonance energy transfer (Table 1)]. Although these "spectroscopic rulers" measure in nanoseconds and nanometers, they can be applied in principle to

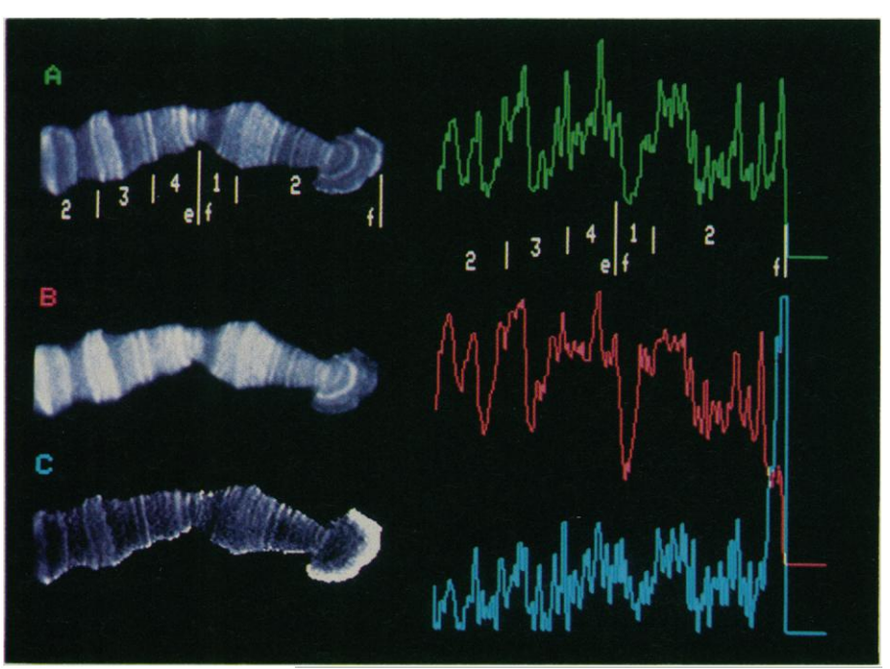

Fig. 4. Localization of AC-rich left-handed Z-DNA sequences in polytene chromosomes of *Chironomus thummi* by GIPS image analysis of triple-stained preparations. The left end of chromosome II region e2-f2 according to Keyl (*50*) is shown, with map designations displayed below the chromosome. Images (left) were averaged over 256 successive frames (frequency, 25 Hz), with background subtracted and normalized (contrast stretched). The gray-level distribution along a cursor line tracing the chromosomal axis is displayed on the right for each image. (A) Polyclonal rabbit antibody Z6, which binds either GC- or AC-rich DNA sequences in the left-handed conformation: indirect staining with fluorescein-labeled goat antibody to rabbit immunoglobulin G (IgG) (green emission). (B) Saturating amounts of D11, a monoclonal antibody to left-handed Z-DNA with specificity for $d(G\text{-}C)_n$: indirect staining with Texas-red–labeled goat antibody to mouse IgG (red emission). The monoclonal antibody was in great excess. (C) Arithmetic ratio (A:B) of images A and B brought into register (usually achieved by adjusting the stage while displaying the B–A difference image during acquisition or image translations during processing). The scaling in the line scan of the ratio image is amplified to depict small fluctuations in the distribution outside the telomere. The telomere under these conditions is off-scale by a factor of 6. The data were collected with GIPS (Fig. 1) with an epi-illumination Zeiss fluorescence microscope with 50-W mercury arc lamp excitation:oil immersion 63X objective (NA, 1.4); Zeiss excitation and emission filters with additional neutral density filters in the excitation beam; COHU 4410 TV camera. [For characterization of the antibodies and detailed materials and methods, see (*45, 46*).] The distribution of right-handed B-DNA assessed by the blue-emitting dye H-33342 is not shown.

each pixel or neighborhood making up the image. The relevant software in this and related instances should include explicit consideration of the underlying photophysical and chemical principles governing molecular processes in solution and in condensed phases (*1*). The images derived no longer depict the mere localization of substances within the physical object but rather the spatial distribution of functional attributes.

Applications

Kinetic processes in living cells. An understanding of many cellular functions requires correlated quantification, morphological localization, and temporal information derived from living cells. In most cases the desired quantification involves combined operations on more than one image, a task for which F-DIM is ideally suited.

Cultured rat myoblasts grown to confluence become committed to terminal differentiation, resulting in fusion into large multinucleated myotubes. An early step in this commitment is the cessation of DNA replication and cell division. After this step but before myoblast fusion, receptor-mediated uptake of α_2-macroglobulin ceases (*41*). Thus living cells in confluent culture can be assigned a position in the process of commitment according to their ability to accumulate rhodamine-labeled α_2-macroglobulin in intracellular vesicles. These cells can be further characterized for other differentiation markers with monoclonal antibodies to developmentally regulated cellular components. We have used F-DIM in such a study. Figure 2 demonstrates that nonarrested cells can be distinguished from cells about to undergo fusion or from those already in myotubes by their uptake of α_2-macroglobulin. Excess free ligand in the surrounding medium obscures normal visualization of the process, but this can be suppressed with F-DIM by subtraction of the fluorescence image at time zero.

Dynamic regulation of compartmentalized ion concentrations is involved in a number of complex cellular functions. The changes are particularly important in contractile cells but have been difficult to measure in single smooth muscle fibers because of the small size of the cells. Figure 3A shows two photomicrographs of such cells before and after brief extracellular electrical stimulation (*42*). The dye, Fura2, exhibits large changes in excitation spectrum and fluorescence quantum efficiency upon binding Ca^{2+}. With F-DIM, the intracellular distribution of Fura2 and thus free Ca^{2+} can be assessed with a spatial resolution of 0.25 μm (*5*). In Fig. 3B, the contour image of *p*Ca (log[Ca^{2+}]) in a resting muscle cell has been calculated from the ratio of emission above 500 nm by excitation at 340 and 380 nm. The results, based on image ratios, are independent of variations in local dye concentration and cell geometry. The distribution of free Ca^{2+} is not uniform; regions adjoining the cell membrane (probably the sarcoplasmic reticulum) and in the cell nucleus show a higher concentration than the rest of the cytoplasm (*5*). Upon induction of cell contraction by electrical stimulation or carbachol administration, the concentration of free Ca^{2+} in the cytoplasm rises while that in the nucleus remains unchanged.

Cellular processes involving macromolecular assembly can be studied in situ by combining F-DIM with fluorescence recovery after photobleaching (DIM-FRAP) (*43*). For example, the direction and mechanism of microtubule polymerization have been inferred from

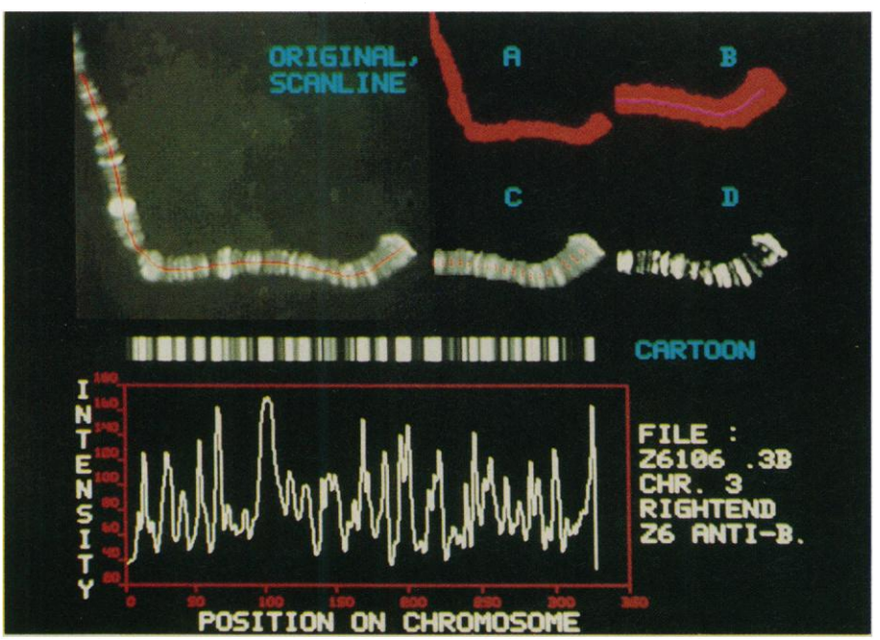

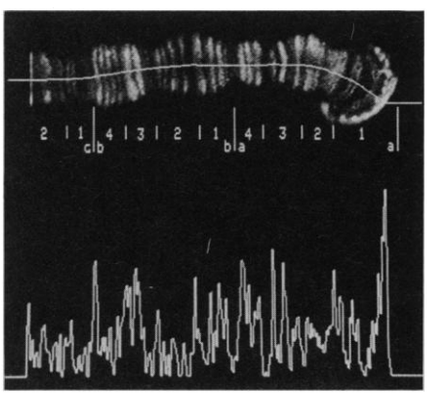

Fig. 5. Quantification, rectification, and linear representation of fluorescence images of *C. thummi* chromosome III (stained with Z6 antibody as in Fig. 4) using the DIP system. A software package was developed by Nederlof to obtain quantitative distributions and linear representations of left-handed DNA in *C. thummi* polytene chromosomes from immunofluorescence images. The image was generated as in Fig. 4, recorded on video tape, and digitized by DIP (*40*). Upper left panel is the original video image with a superimposed smoothed and extrapolated scan line (skeleton). (A) Binary mask of the chromosome generated by calculating a threshold from the image histogram; (B) part of the mask showing the skeleton created by erosion with shape preservation; (C) the image after background subtraction, with some of the lines perpendicular to the skeleton used for calculating an average scan line (the latter requiring bilinear interpolation in regions of chromosome bending); (D) the enhanced chromosome image after contrast stretching and normalization of the mask with the mean scan-line value. Cartoon: a straight and enhanced bar representation of the original image (contrast stretched and median filtered as in D). Lower panel is a plot of the intensities in the enhanced image over the 5-pixel thick scan line. This method provides a means by which all chromosomes of a similar class may be compared according to their immunofluorescence distribution. Fig. 6. Laser-scanning fluorescence imaging. The image was acquired with a Zeiss LSM in combination with GIPS. Staining was with the polyclonal Z6 antibody as in Fig. 4. The right-hand end of *C. thummi* chromosome I region Ia1-Ic2 is shown. LSM settings: argon laser 488-nm excitation; attenuator setting, 5; oil immersion 63X objective (NA, 1.4); scan time, 8 seconds; zoom magnification, 25X. (Upper panel) Image with cursor line positioned parallel to the central axis of the chromosome; (lower panel) gray-level intensity distribution along cursor line.

the repopulation of assembled microtubules with fluorescent-labeled tubulin after spot photobleaching. DIM-FRAP measurements have ruled out the treadmill hypothesis, that is, a mechanism involving the addition of monomer subunits at the spindle equator and loss of monomers at the pole ends (*9*).

Finally, we would draw attention to the pioneering efforts in the time-resolved and spatially resolved optical recording of action potentials in single neu-

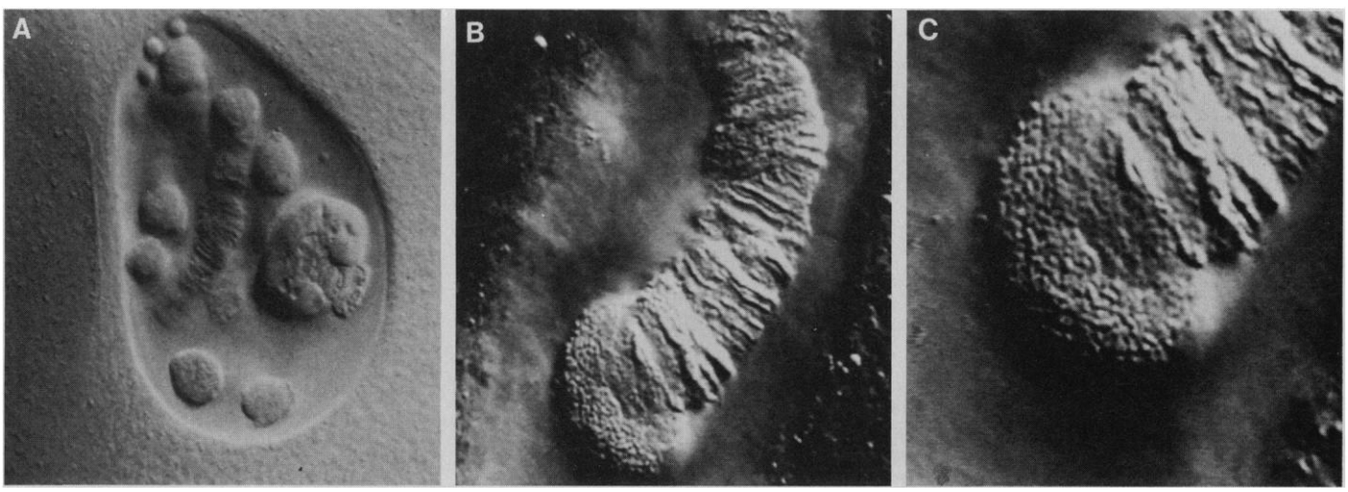

Fig. 7. Laser-scanning differential interference contrast imaging of *C. thummi* polytene chromosomes in whole-mount salivary gland. LSM settings as in Fig. 6 except as follows: attenuator setting, 3; zoom magnification, 12X (A), 30X (B), 50X (C). (A) An optical cross section of a nucleus within the gland showing the centromere of chromosome IV with the nucleolus and the left end of chromosome I. (B) An optical section of the terminal region of chromosome I at higher magnification. (C) Higher magnification of the telomere with apparent demonstration of higher order chromatin structure (perhaps looping of the chromomeres). The nuclei are about 50 μm in diameter, and the individual chromosomes have a transverse dimension of about 10 μm. Contrast enhancement was electronically controlled, and resolution was 0.5 μm or less throughout.

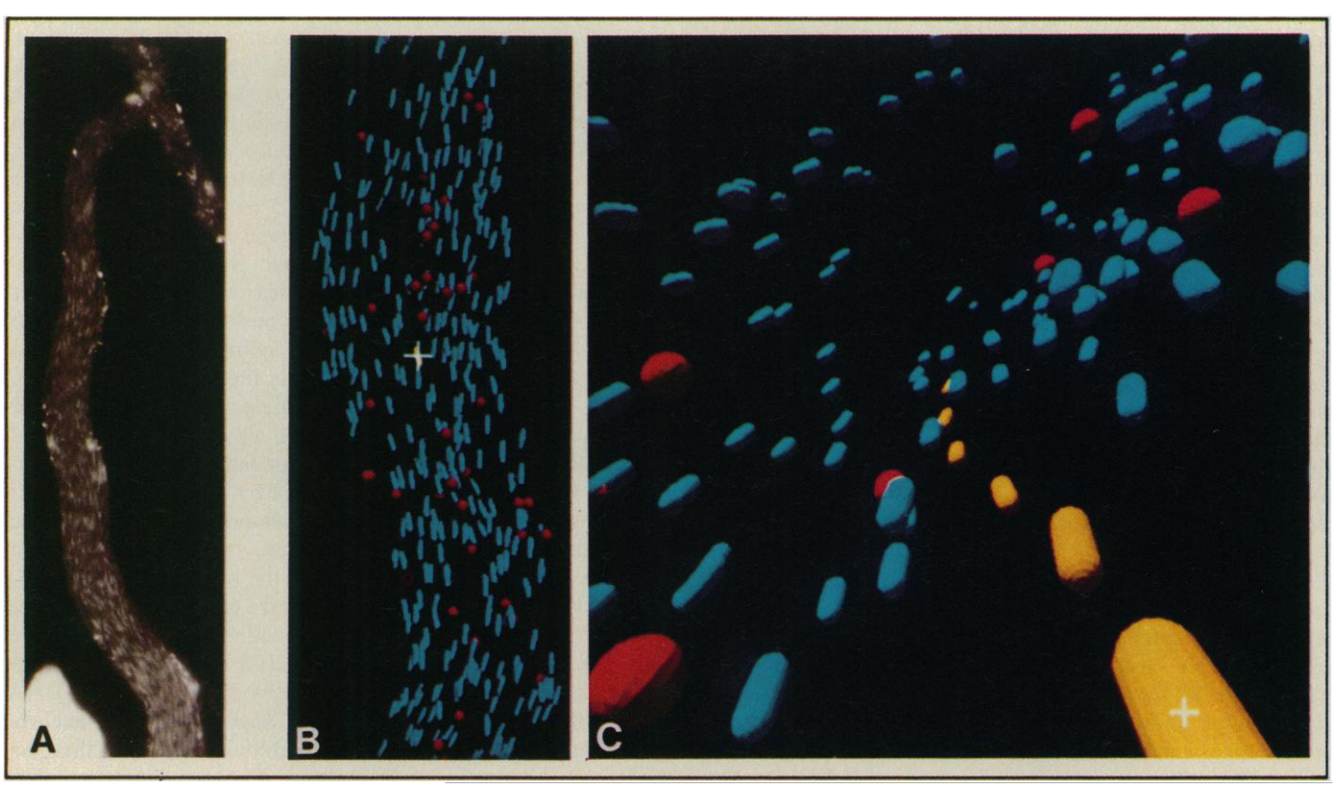

Fig. 8. Distribution of α-actinin in a single smooth muscle cell determined with F-DIM and 3D image reconstruction [data from Fay and colleagues (*47*)]. (A) Digitized fluorescence image of a single optical cross section of a toad muscle stained with rhodamine-labeled antibody to α-actinin. The image is the result of (i) averaging of 128 frames, (ii) subtraction of a background record, (iii) multiplication by a gain normalization "map" to correct for instrumental spatial variations, and (iv) contrast stretching. Two types of bodies can be recognized: a fusiform structure distributed throughout the cytoplasm, and more irregularly shaped plaques associated with the plasma membrane. (B) 3D reconstruction image projected onto a plane in which the blue cylinders indicate the positions and orientations of the fusiform elements and the red spheres indicate the positions of the plaques. The image was corrected for blurring using an iterative restoration algorithm. A filtering method was used to find the centers and orientation of the bodies (*47*). (C) A computer-generated view from inside the cell used in an interactive analysis program to determine patterns of organization among the elements. A directed nearest-neighbor analysis identified successive elements in a string (yellow).

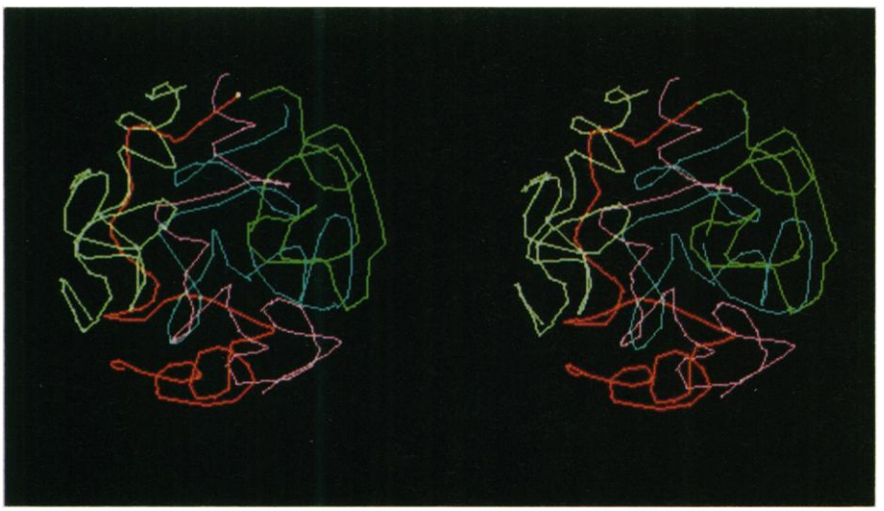

Fig. 9. Stereo pair of the reconstructed folding pattern of polytene chromosomes in a *Drosophila* salivary gland nucleus [data and procedures from Sedat, Agard, and colleagues (*17, 49*)]. The chromosomes are color coded as follows: green, X; orange, 2L; blue, 2R; purple, 3L; light green, 3R. Twenty-four images at successive focus steps (0.2 μm) through a nucleus stained in situ with the DNA-specific fluorescent dye 4′, 6-diimidino-2-phenylindole were digitized and refined to remove out-of-focus information, and the chromosome paths were traced out using an interactive modeling program.

rons and cell populations from high-intensity fluorescence (also absorption and birefringence) signals derived from impermeant dyes sensitive to membrane potential (*44*). Nonintensified photodiode arrays (for example, 10 by 10 elements) with parallel readout have been used to register the small relative signal changes (less than 10^{-3}) associated with excitation and depolarization processes. Whether the other F-DIM techniques can be applied to such studies remains to be established.

Immunofluorescence probes of DNA conformation. In certain studies, a knowledge of the actual distribution of several components within the same biological structure is required. For example, to assess the possible role (or roles) that left-handed Z-DNA (*45*) may have in chromatin structure or gene expression, we need to determine (i) the amount of left-handed DNA in relation to total DNA; (ii) the sequence characteristics of the left-handed DNA loci; and (iii) the local distribution of left-handed DNA sequences along the genetic map. Mono- and polyclonal antibodies specific for left-handed DNA of a particular alternating purine-pyrimidine sequence or family of sequences can be used to acquire this information. Insect polytene chromosomes constitute ideal test objects because of a natural signal enhancement factor and a linear arrangement of the genetic material well matched to the resolution of the light microscope. Polytene chromosomes arise as the result of 9 to 13 rounds of DNA replication without cell division, whereby the individual chromomeres are aligned in register, providing a 200-μm long genetic map in which each gene is represented 8,000 to 16,000 times (rather than twice as in the diploid genome).

Fluorescent-labeled antibodies were used to map DNA tracts with the potential of adopting a left-handed conformation, and total DNA was assessed by the fluorescence of a DNA-specific dye. The three spectrally separated fluorescence images of triple-stained chromosomes were acquired by F-DIM (GIPS system, Fig. 1) with the high-speed ALU processor to enable real-time signal averaging and registration (*46*). Figure 4 illustrates the images and processing used to extract information about the distribution of AC-rich tracts of Z-DNA. From such data we have determined that sequences capable of forming left-handed DNA occur at a frequency of 0.02 to 0.1 percent in almost every gene but at a higher frequency in the strongly heterochromatic regions of the chromosome involved in ectopic pairing (*45, 46*). Saturation of left-handed GC-rich tracts by the monoclonal antibody (Fig. 4B) leads to a predominant staining of the telomeres of the three large chromosomes by the polyclonal antibody, which recognizes both $d(G\text{-}C)_n$ and $d(A\text{-}C)_n \cdot d(G\text{-}T)_n$ alternating purine-pyrimidine left-handed sequences. We conclude that AC-rich tracts occur in these telomeres at a frequency 25 times greater than that in adjacent regions.

To assess the influence of environmental factors (*p*H, ionic strength, and temperature), transcriptional activity, and treatments such as fixation on the ability of the antibodies to recognize left-handed sequences, we require fluorescence profiles of the chromosomes free of distortions caused by variations in shape, stretching, and orientation. Nederlof, using the Delft Image Processor (DIP) (*40*), has been able to generate such representations by the image processing procedures described in Fig. 5.

Image reconstruction. There are several instruments with which optical sectioning (*15–17*) for the purposes of 3D reconstruction can be accomplished: laser scanning microscopes (LSM), fluorescence or bright-field optical sectioning microscopes (OSM), and differential interference contrast microscopes (DICM).

The type 2 LSM (*15*) produces 2D images with the least out-of-focus information because the point spread function is determined by two confocal objectives with high numerical aperture, which focus a point source on the object while the emitted or transmitted light is focused through a pinhole on the detector. An image is built up by scanning the source and detector in synchrony. Little or no mathematical correction need be applied to reconstruct 3D images. Wijnaendts van Resandt and coworkers (*21*) have designed an instrument in which the laser illumination and optical system are stationary and the object is translated in three dimensions. The resolution achieved in fluorescence is 0.9 μm in the *z* axis and 0.25 μm in the object plane with a rhodamine fluorophore and 514-nm argon laser excitation; the corresponding values with a 285-nm laser source are 0.5 and 0.1 μm. In a type 1b LSM (*15*) the point-source illumination of the object is the same as for type 2, but an area detector (photomultiplier) measures the emission intensity relayed by the collector lens. In such an instrument described by Wilke (*22*), the laser excitation and fluorescence emission are galvanometrically scanned through two dimensions in the object plane.

We have used a commercial Zeiss type 1b LSM to generate images that were analyzed by GIPS to determine the distribution of antibody to left-handed DNA bound to the *Chironomus* polytene chromosomes, material similar to that described above. Figure 6 shows a typical image and its corresponding line histogram. The resolution is superior to that achieved with an arc lamp light source and TV camera sensor. The laser spot illumination leads to a great reduction in fluorescence flare and scattering.

The ability of laser scanning systems to obtain clearly focused sections of

thick specimens is demonstrated by the same Zeiss LSM in the DICM mode (Fig. 7). The polytene chromosomes within a whole explanted *Chironomus* salivary gland are clearly visible at high resolution (less than 0.25 μm), even though the specimen has a thickness greater than 40 μm.

Most 3D image reconstructions of biological specimens from the light microscope have been generated by the combined use of OSM and F-DIM. The images are processed mathematically to eliminate out-of-focus contributions (*17, 18, 28, 47–49*). Fay and coworkers have undertaken an analysis of the molecular basis and organization of the contractile apparatus in smooth muscle cells by studying the distribution of fluorescent-labeled antibody to the protein α-actinin (*47*). The α-actinin bodies appear to anchor oppositely directed, thin, actin-containing filaments; the direction of the α-actinin bodies may indicate the lines of force in the contractile apparatus. Figure 8 illustrates (A) a single optical cross section, (B) a 3D image of the distribution and orientation of bodies rich in α-actinin, and (C) a computer-generated view from inside the cell. The strings of elements identified by this reconstruction appear to be loci for the generation of force; they terminate at the larger spherical elements along the cell membrane and shorten during active contraction.

The combined OSM/F-DIM method has been applied to *Drosophila* salivary gland nuclei labeled with a DNA-specific fluorescent dye to determine the spatial organization of the polytene chromosomes (*17, 48, 49*). In this case, the 2D images were arranged into a 3D representation by interactive analysis (Fig. 9). By comparing 24 reconstructed nuclei (like the one shown in Fig. 9) from 5 larvae, general features were extracted. The methods used for comparison define the path of the chromosomes in quantitative terms by creating function plots such as (i) the distance between 20 to 30 selected bands on each chromosome, (ii) the distance between selected points along the chromosome path and the nuclear envelope, and (iii) the overall geometric curvature of each chromosome path. Plots of these functions for the same chromosome from different nuclei can be overlaid and an average envelope calculated (*49*). Invariant properties were found to be the separation of chromosome arms into exclusive spatial domains and adhesion of the chromocenter to the nuclear envelope. Features that occurred in many but not all nuclei included right-handed chromosome coiling, orientation of the telomeres at one end and the centromeres at the opposite pole, and apposition of the nuclear envelope close to the chromosomes at regions of intercalated heterochromatin.

Conclusion

It can be anticipated that DIM in general and F-DIM in particular will be increasingly adopted by cell biologists as a valuable tool in studies of complex cellular functions and higher order structure. Further technological developments alluded to in this paper, as well as others not mentioned, should provide the even greater versatility required for the next generation of biochemical and molecular biological probes.

References and Notes

1. G. Weber, in *Applications of Fluorescence in the Biomedical Sciences*, D. L. Taylor, A. S. Waggoner, F. Lanni, R. Murphy, R. Birge, Eds. (Liss, New York, in press).
2. L. Ornstein, W. Mautnew, B. J. Davis, R. Tamura, *J. Mt. Sinai Hosp.* **24**, 1066 (1957); D. L. Taylor and Y.-L. Wang, *Nature (London)* **284**, 405 (1980).
3. R. E. Smith and F. A. Dolbeare, in *Flow Cytometry*, M. Melamed, P. Mullaney, M. Mendelsohn, Eds. (Wiley, New York, 1979), p. 317; F.A. Dolbeare in *Modern Fluorescence Spectroscopy*, A. Wehry, Ed. (Plenum, New York, 1981), vol. 3, p. 251.
4. On *p*H, see L. Tanasugarn, P. McNeil, G. T. Reynolds, D. L. Taylor, *J. Cell Biol.* **98**, 717 (1984). On membrane potential dyes, see L. V. Johnson, M. L. Walsh, B. J. Bockus, L. B. Chen, *ibid.* **88**, 526 (1981); R. L. Cohen, K. A. Muirhead, J. E. Gill, A. S. Waggoner, P. K. Horan, *Nature (London)* **290**, 593 (1981); A. S. Waggoner, in *The Enzymes of Biological Membranes*, A. Martinosi, Ed. (Plenum, New York, 1985), vol. 1, p. 313.
5. D. A. Williams and F. S. Fay, *Biophys. J.* **47**, 131a (1985); D. M. Williams, K. Fogarty, R. Y. Tsien, F. S. Fay, *Nature (London)*, in press.
6. I. H. Pastan and M. C. Willingham, *Annu. Rev. Physiol.* **43**, 239 (1981); B. Herman and D. F. Albertini, *J. Cell Biol.* **98**, 565 (1984); M. W. Berns, A. E. Siemens, R. J. Walter, *Cell Biophys.* **6**, 263 (1984).
7. G. Koehler and C. Milstein, *Nature (London)* **256**, 495 (1975).
8. Y.-L. Wang, J. Heiple, D. L. Taylor, *Methods Cell Biol.* **24B**, 1 (1982); D. L. Taylor, P. A. Amato, K. Luby-Phelps, P. McNeil, *Trends Biochem. Sci.* **9**, 88 (1984).
9. On α-actinin, see J. R. Feramisco, *Proc. Natl. Acad. Sci. U.S.A.* **76**, 3967 (1979). On actin-binding peptides, see J. E. Kreis, K. H. Winterhalter, W. Birchmeier, *ibid.*, p. 3814; E. Wulf, A. Deboben, F. A. Bautz, H. Faulstich, T. Wieland, *ibid.*, p. 4498. On tubulin probes, see Clark and D. Garland, *J. Cell Biol.* **76**, 619 (1978); M. Zavortink, M. J. Welsch, J. R. McIntosh, *Exp. Cell Res.* **149**, 375 (1983); J. R. McIntosh, W. M. Saxton, D. L. Stemple, R. J. Leslie, M. J. Welsh, *Ann. N.Y. Acad. Sci.*, in press; P. Wadsworth and E. D. Salmon, private communication.
10. M. C. Willingham and I. Pastan, *Cell* **13**, 501 (1978); F. R. Maxfield, J. Schlessinger, Y. Schechter, I. Pastan, M. C. Willingham, *ibid.* **14**, 805 (1978); H. T. Haigler, J. F. Ash, S. J. Singer, S. Cohen, *Proc. Natl. Acad. Sci. U.S.A.* **75**, 3317 (1978); M. C. Willingham and I. H. Pastan, *Methods Enzymol.* **98**, 266 (1983); W. W. Webb, in *Applications of Fluorescence in the Biomedical Sciences*, D. L. Taylor, A. S. Waggoner, F. Lanni, R. Murphy, R. Birge, Eds. (Liss, New York, in press).
11. T. Hirschfeld, *Appl. Opt.* **15**, 2965 (1976). On single molecule detection in liquids, see N. J. Dovichi, J. C. Martin, J. H. Jett, M. Trkula, R. A. Keller, *Anal. Chem.* **56**, 348 (1984).
12. A. N. Glazer and L. Stryer, *Trends Biochem. Sci.* **12**, 423 (1984). For a comprehensive structural and bibliographic survey of spectroscopic probes, see R. Haughland, *Handbook of Fluorescent Probes and Research Chemicals* (Molecular Probes, Inc., Junction City, Ore., 1985).
13. See Reynolds in (*63*); more recently, Y. Talmi, *Multichannel Image Detectors* (American Chemical Society, Washington, D.C., 1983), vol. 2; J. G. Timothy, *Publ. Astron. Soc. Pacific* **95**, 810 (1983); G. T. Reynolds and D. L. Taylor, *BioScience* **30**, 586 (1980).
14. I. T. Young, D. L. Dunbar Balasubramanian, R. L. Peverini, R. P. Bishop, *IEEE Trans. Biomed. Eng.* **29**, 70 (1982); M. Lampton, *Sci. Am.* **245**, 46 (November 1981).
15. T. Wilson and C. Sheppard, *Theory and Practice of Scanning Optical Microscopy* (Academic Press, New York, 1984).
16. E. A. Ash, *Scanned Image Microscopy* (Academic Press, New York, 1980).
17. D. A. Agard, *Annu. Rev. Biophys. Bioeng.* **13**, 191 (1984).
18. E. R. Macagno, C. Levinthal, I. Sobel, *ibid.* **8**, 323 (1979); N. Streibl, *J. Opt. Soc. Am. A* **2**, 121 (1985).
19. F. Lanni, in *Applications of Fluorescence in the Biomedical Sciences*, D. L. Taylor, A. S. Waggoner, F. Lanni, R. Murphy, R. Birge, Eds. (Liss, New York, in press).
20. G. J. Brakenhoff, P. Blom, P. Barends, *J. Microsc.* **117**, 219 (1979); G. J. Brakenhoff, *ibid.*, p. 233; R. Shoemaker, D. W. Hillman, J. Jonas, D. Kessler, R. V. Shack, D. Vukobratovich, *IEEE Trans. Biomed. Eng.* **29**, 82 (1982).
21. R. W. Wijnaendts van Resandt, H. J. B. Marsman, R. Kaplan, J. Davoust, E. H. K. Stelzer, R. Striker, *J. Microsc.*, **138**, 29 (1984).
22. V. Wilke, *Scanning* **7**, 88 (1985).
23. I. T. Young, *Proc. Int. Soc. Opt. Eng.* **397**, 326 (1983).
24. For a discussion of sampling error estimation, see Letters to the Editor, *Cytometry* **6**, 273 (1985).
25. M. Kerker, *Cytometry* **4**, 1 (1984); M. Kerker *et al.*, *ibid.* **3**, 71 (1982); T. P. Burghardt and N. L. Thompson, *Biophys. J.* **47**, 729 (1984).
26. S. Matsumoto, K. Morikawa, K. Yanagida, *J. Mol. Biol.* **152**, 501 (1981); M. Yanagida, Y. Hiraoka, I. Katsura, *Cold Spring Harbor Symp. Quant. Biol.* **47**, 177 (1983).
27. A. Lewis, M. Isaacson, A. Harootunian, A. Muray, *Ultramicroscopy* **13**, 227 (1984); E. Betzig, A. Lewis, A. Harootunian, M. Isaacson, E. Kratschmer, in preparation.
28. K. R. Castleman, *Digital Image Processing* (Prentice-Hall, Englewood Cliffs, N.J., 1979).
29. D. J. Arndt-Jovin and T. M. Jovin, *Annu. Rev. Biophys. Bioeng.* **7**, 527 (1978); T. M. Jovin and D. J. Arndt-Jovin, *Trends Biochem. Sci.* **8**, 214 (1980); M. Melamed, P. Mullaney, M. Mendelsohn, *Flow Cytometry and Sorting* (Wiley, New York, 1979).
30. On imaging of whole cells with array and multiwavelength emission detection, see L. S. Cram, M. F. Bartholdi, L. L. Wheeless, J. W. Gray, in *Flow Cytometric Instrumentation and Data Analysis*, M. A. Van Dilla, P. N. Dean, O. D. Laerum, M. R. Melamed, Eds. (Academic Press, Orlando, 1985), p. 161.
31. R. D. McCorkle, J. Angilello, G. Coleman, R. Feder, S. J. La Placa, *Science* **205**, 401 (1979); R. Feder *et al.*, *ibid.* **227**, 63 (1984); G. Schmahl and D. Rudolph, Eds., *X-Ray Microscopy* (Springer-Verlag, Berlin, 1984).
32. O. H. Griffith, G. F. Rempfer, K. K. Nadakavukaren, in *Electron Microscopy*, J. B. Le Poole, Ed. (Deutsche Gesellschaft Electronenmikroskopie, Frankfurt, 1982), vol. 1, p. 59; K. K. Nadakavukaren, L. B. Chen, D. L. Habliston, O. H. Griffith, *Proc. Natl. Acad. Sci. U.S.A.* **80**, 4012 (1983); O. H. Griffith and G. B. Birrell, *Trends Biochem. Sci.* **10**, 336 (1985).
33. S. Chandra and G. H. Morrison, *Science* **228**, 1543 (1985).
34. G. Binnig and H. Rohrer, *Sci. Am.* **253**, 40 (August 1985); A. M. Baro *et al.*, *Nature (London)* **315**, 253 (1985).
35. See R. Lewis, *Electronic Imaging* (January 1985), p. 44; I. Hirschberg, *ibid.* (April 1985), p. 56.
36. J. G. Timothy, *IEEE Trans. Nuclear Sci.*, in press; see also Timothy in (*13*).
37. H. Harms and H. M. Aus, *Cytometry* **5**, 236 (1984); recently 11 algorithms for autofocusing have been compared for use with video imaging [F. C. A. Groen, I. T. Young, G. Ligthart, *ibid.* **6**, 81 (1985)].
38. M. Onoe, K. Preston, Jr., A. Rosenfeld, *Real-Time Medical Image Processing* (Plenum, New York, 1980); T. M. Cannon and B. R. Hunt, *Sci. Am.* **245**, 136 (October 1981); K. Preston, Jr., K. J. W. Taylor, S. A. Johnson, W. R. Ayers, *Medical Imaging Techniques, A Comparison* (Plenum, New York, 1979); R. C. Gonzalez and P. Wintz, *Digital Image Processing* (Addison-

Wesley, Reading, Mass., 1977); W. K. Pratt, *Digital Imaging Processing* (Wiley, New York, 1978).
39. W. T. Cathey, B. R. Frieden, W. T. Rhodes, C. K. Rushforth, *J. Opt. Soc. Am. A* **3**, 241 (1984).
40. M. J. B. Duff, Ed. *Computing Structures for Image Processing* (Academic Press, London, 1983); D. A. Symanow, D. J. Svetkoff, P. F. Leonard, *Electronic Imaging*, 46 (February, 1985). On the Delft image analysis laboratory system, see F. A. Gerritsen, thesis, Technical University of Delft, Delft, Netherlands (1982); R. P. W. Duin, in *Computing Structures for Image Processing*, M. J. B. Duff, Ed. (Academic Press, London, 1983), p. 141.
41. S. J. Kaufman *et al.*, *Exp. Cell Res.* **25**, 333 (1980); K. R. Haye, R. F. Foster, S. J. Kaufman, *J. Cell Biol.* **99**, 312a (1984); S. J. Kaufman and R. Robert-Nicoud, *Cytometry*, in press.
42. F. S. Fay and C. M. Delise, *Proc. Natl. Acad. Sci. U.S.A.* **70**, 641 (1973).
43. D. Axelrod, D. E. Koppel, J. Schlessinger, E. L. Elson, W. W. Webb, *Biophys. J.* **16**, 1055 (1976); D. E. Koppel, *ibid.* **28**, 281 (1979); G. M. McGregor, H. G. Kapitza, K. A. Jacobsen, *Laser Focus*, 85 (November 1984); H. G. Kapitza, G. McGregor, K. A. Jacobsen, *Proc. Natl. Acad. Sci. U.S.A.* **82**, 4122 (1985).
44. B. M. Salzberg, in *Current Methods in Cellular Neurobiology*, J. L. Barker, Ed. (Wiley, New York, 1983), p. 139; A. Grinvald, *Annu. Rev. Neurosci.* **8**, 263 (1985).
45. T. M. Jovin *et al.*, *Cold Spring Harbor Symp. Quant. Biol.* **47**, 143 (1983); D. A. Zarling, D. J. Arndt-Jovin, M. Robert-Nicoud, R. Thomae, L. P. McIntosh, T. M. Jovin, *J. Mol. Biol.* **176**, 369 (1984); D. J. Arndt-Jovin, M. Robert-Nicoud, D. A. Zarling, C. Greider, E. Weimer, T. M. Jovin, *Proc. Natl. Acad. Sci. U.S.A.* **80**, 4344 (1983).
46. D. J. Arndt-Jovin, M. Robert-Nicoud, P. Baurschmidt, T. M. Jovin, *J. Cell Biol.*, in press.
47. F. S. Fay, R. T. Fujiwara, K. Fogarty, D. J. Rees, *Cell Biol.* **96**, 783 (1983); F. S. Fay, K. E. Fogarty, J. M. Coggins, in *Optical Methods in Cell Physiology*, P. DeWeer and B. Salzburg, Eds. (Wiley, New York, in press).
48. D. A. Agard and J. W. Sedat, *Nature (London)* **302**, 676 (1983); D. Mathog, M. Hochstrasser, J. W. Sedat, *J. Microsc.* **137**, 241 (1985).
49. D. Mathog, M. Hochstrasser, Y. Gruenbaum, H. Saumweber, J. Sedat, *Nature (London)* **308**, 414 (1984); Y. Gruenbaum, M. Hochstrasser, D. Mathog, H. Saumweber, D. A. Agard, J. W. Sedat, *J. Cell Sci. Suppl.* **1**, 223 (1984); D. Mathog, *J. Microsc.* **137**, 253 (1985); M. Hochstrasser, D. Mathog, Y. Gruenbaum, H. Saumweber, J. W. Sedat, *J. Cell. Biol.*, in press.
50. H.-G. Keyl, *Chromosoma* **8**, 739 (1957).
51. The references to actual or proposed implementation with digital and other image processing techniques are deemed to be representative and current but do not constitute a comprehensive survey of the relevant literature.
52. H. Piller, *Microscope Photometry* (Springer, Berlin, 1977).
53. R. D. Allen, J. L. Travis, N. S. Allen, H. Yilmay, *Cell Motility* **1**, 275 (1981); R. J. Walter and M. W. Berns, *Proc. Natl. Acad. Sci. U.S.A.* **78**, 6927 (1981); K. Yamamoto and A. Taira, *J. Microsc.* **129**, 49 (1983).
54. R. D. Allen and N. S. Allen, *J. Microsc.* **129**, 3 (1983).
55. J. S. Ploem, *Z. Wiss. Mikr.* **68**, 129 (1967).
56. J. A. Dvorak, L. H. Miller, W. C. Whitehouse, T. Shiroishi, *Science* **187**, 748 (1975); R. D. Allen, N. S. Allen, J. L. Travis, *Cell Motility* **1**, 291 (1981); S. Inoue, *J. Cell Biol.* **89**, 346 (1981); K. R. Spring, *Pfluegers Arch.*, in press.
57. D. Keller, C. Bustamante, M. F. Maestre, I. Tinoco, Jr., *Proc. Natl. Acad. Sci. U.S.A.* **82**, 401 (1985).
58. W. Mickols, J. E. Katz, M. F. Maestre, I. Tinoco, Jr., C. Bustamante, *Rev. Sci. Instrum.*, in press; W. Mickols, M. F. Maestre, I. Tinoco, Jr., S. H. Embury, *Proc. Natl. Acad. Sci. U.S.A.*, in press.
59. B. Kachar, *Science* **227**, 766 (1985); *ibid.*, p. 1355; C. J. R. Sheppard and D. K. Hamilton, *Appl. Optics* **22**, 886 (1983).
60. D. Axelrod, *Cell Biophys.* **3**, 167 (1981); R. N. Smartt and W. H. Steel, *Appl. Opt.* **24**, 1402 (1985).
61. G. W. Ellis, in *ICN–UCLA Symposium on Molecular and Cellular Biology*, E. R. Dirksen, D. M. Prescott, C. F. Fox, Eds. (Academic Press, New York, 1978), vol. 12, p. 465.
62. C. J. R. Sheppard and R. Kompfner, *Appl. Opt.* **17**, 2879 (1978); see also (*15*).
63. G. T. Reynolds, *Q. Rev. Biophys.* **5**, 295 (1972); I. Pastan, W. W. Webb, E. L. Elson, *Proc. Natl. Acad. Sci. U.S.A.* **74**, 2909 (1977); J. Schlessinger, Y. Schechter, M. Willingham, I. Pastan, *ibid.* **75**, 2659 (1978).
64. J. W. MacInnes and R. B. Uretz, *Science* **151**, 689 (1966); G. V. Sengbusch and A. Thaer, in *Fluorescence Techniques in Cell Biology*, A. A. Thaer and M. Sernetz, Eds. (Springer, Berlin, 1973), p. 31; T. M. Jovin, in *Flow Cytometry*, M. Melamed, P. Mullaney, M. Mendelsohn, Eds. (Wiley, New York, 1979), p. 137; J. E. Solomen, *Appl. Opt.* **20**, 1537 (1981).
65. S. M. Fermandez and R. D. Berlin, *Nature (London)* **264**, 411 (1976); L. Trón *et al.*, *Biophys. J.* **45**, 939 (1984).
66. D. J. Arndt-Jovin, S. A. Latt, G. Striker, T. M. Jovin, *J. Histochem. Cytochem.* **27**, 87 (1979).
67. T. Hirschfeld, *Can. J. Spectrosc.* **10**, 128 (1965); D. Axelrod, *J. Cell Biol.* **89**, 141 (1981); D. Axelrod, T. P. Burghardt, N. L. Thompson, *Annu. Rev. Biophys. Bioeng.* **13**, 247 (1984); F. Lanni, A. S. Waggoner, D. L. Taylor, *J. Cell Biol.* **100**, 1091 (1985).
68. P. Johnson and P. B. Garland, *FEBS Lett.* **132**, 252 (1981); *Biochem. J.* **203**, 313 (1982).
69. We thank K. Spring for helpful discussions and assistance with reference material; F. S. Fay, J. W. Sedat, and M. Nederlof for providing data and figures included in this article; I. T. Young for helpful discussions and collaborations; H. Epelbaum for assistance in producing the figures; and V. Wilke and the Carl Zeiss Company for the loan of a prototype laser scan microscope. Supported by the Max Planck Society and the German Research Council. S. J. Kaufman was supported as a Senior International Fellow by grant FO6 TWOO960 from the Fogarty International Center of the National Institutes of Health. T. M. Jovin was a Fogarty Scholar-in-Residence at NIH during the compilation of this manuscript.

Time-Resolved Electron Energy Loss Spectroscopy

T. H. Ellis, L. H. Dubois, S. D. Kevan, M. J. Cardillo

In the past two decades, powerful techniques have been developed to study in detail the static properties of simple, well-defined surfaces. A good foundation is now being laid in understanding surface geometries, electronic structures, and vibrational frequencies (*1–3*). The elucidation of elementary surface rate processes is a more complex endeavor, however, and less progress has been made toward this goal (*4–6*). Despite the fact that numerous technologically important processes such as electronic materials growth and processing, heterogeneous catalysis, and corrosion are governed by surface kinetics, a suitable surface probe of rate processes that possesses sufficient dynamic range and chemical sensitivity to yield useful kinetic information has not yet been developed.

Two recent developments in the experimental technique of electron energy–loss spectroscopy (EELS)—dispersion compensation (*7*) and parallel detection (*8*)—have led to the measurement of surface vibrational spectra with a signal strength several orders of magnitude higher than the strength in conventional systems. This increased signal strength permits the measurement of the rates of surface processes on the millisecond time scale, thereby making possible time-resolved EELS (TREELS).

The exploitation of TREELS will significantly expand the capabilities of both thermal desorption spectroscopy and molecular-beam surface scattering. These latter techniques have provided useful kinetic information in the past (*4–6*), but they have been limited to detection of gas-phase products only (that is, they observe the final result of a series of elementary reaction steps on the surface rather than the individual steps themselves).

While the possibilities presented by TREELS are as broad as chemistry itself, four of them have special relevance to both fundamental and applied research:

1) Time-resolved adsorption studies can measure the dynamic properties of metastable precursor and nonequilibrium adsorption states, as well as the dependence of the sticking probability on the incident particle and substrate properties (*9–12*). In addition, sensitive, time-resolved studies will allow investi-

T. H. Ellis is a Natural Sciences and Engineering Research Council of Canada postdoctoral fellow, L. H. Dubois is a member of the technical staff in the Physical and Inorganic Chemistry Department, S. D. Kevan is a member of the technical staff in the Condensed State Physics Department, and M. J. Cardillo is head of the Chemical Physics Department, AT&T Bell Laboratories, Murray Hill, New Jersey 07974.